Research Square

Preprints are preliminary reports that have not undergone peer review.
They should not be considered conclusive, used to inform clinical practice,
or referenced by the media as validated information.

Small reorganization energy acceptors enable low energy losses in non-fullerene organic solar cells

Yanan Shi
National Center for Nanoscience and Technology
Yilin Chang
National Center for Nanoscience and Technology
Kun Lu
National Center for Nanoscience and Technology https://orcid.org/0000-0002-3403-2516
Zhihao Chen
Shandong University
Jianqi Zhang
National Center for Nanoscience and Technology https://orcid.org/0000-0002-3549-1482
Yangjun Yan
National Center for Nanoscience and Technology
Dingding Qiu
National Center for Nanoscience and Technology
Yanan Liu
National Center for Nanoscience and Technology
Muhammad Abdullah Adil
National Center for Nanoscience and Technology https://orcid.org/0000-0002-7658-5370
Wei Ma
Xi'an Jiaotong University https://orcid.org/0000-0002-7239-2010
Xiaotao Hao
Shandong University
Lingyun Zhu
National Center for Nanoscience and Technology https://orcid.org/0000-0001-7391-1866
Zhixiang Wei (weizx@nanoctr.cn)
National Center for Nanoscience and Technology https://orcid.org/0000-0001-6188-3634

Article

Keywords: non-fullerene acceptors, reorganization energy, energy losses, molecular stacking, organic solar cells

Posted Date: December 22nd, 2021

DOI: https://doi.org/10.21203/rs.3.rs-1137629/v1

License: This work is licensed under a Creative Commons Attribution 4.0 International License. Read Full License

Version of Record: A version of this preprint was published at Nature Communications on June 7th, 2022. See the published version at https://doi.org/10.1038/s41467-022-30927-y.

Abstract

Minimizing the energy loss is of critical importance in the pursuit of attaining high-performance organic solar cells (OSCs). Interestingly, electron-vibration coupling (namely reorganization energy) plays a crucial role in the photo-electric conversion processes. However, a molecular understanding of the relationship between the reorganization energy and the energy loss has rarely been studied. Here, two new acceptors Qx-1 and Qx-2 with quinoxaline (Qx)-containing fused core were designed and synthesized. The results indicate that the reorganization energies of these two acceptors during the photoelectric conversion processes are substantially smaller than the conventional Y6 acceptor, which is beneficial for improving the exciton lifetime and diffusion length, promoting charge transport and reducing the energy loss originating from exciton dissociation and non-radiative recombination. As a result, an outstanding power conversion efficiency (PCE) of 18.2% with high V_{oc} above 0.93 V in the PM6:Qx-2 blend, accompanying a significantly reduced energy loss of 0.48 eV. To the best of our knowledge, the obtained energy loss is the smallest for the binary OSCs with PCEs over 16% reported to date. This work underlines the importance of the reorganization energy in achieving small energy loss in organic active materials and paves a new way to obtain high-performance OSCs.

Introduction

In recent years, organic solar cells (OSCs) have gained wide attention on account of being lightweight, solution-processable and for ensuring low-cost large-area and semitransparent flexible thin-film device preparation.[1-5] Owing to great strives in material design and device optimization, [6-9] the power conversion efficiency (PCE) of OSCs based on Y6 nonfullerene acceptors (NFAs) have reached 18% for the binary devices and 19% for the tenary and tandem devices.[10-12] Nonetheless, compared with inorganic and perovskite solar cells, the OSCs photovolatic performance still lag behind due to the relatively greater energy losses. [13-16] Currently, the open circuit voltage (V_{oc}) of most high-performance OSCs is still limited to 0.8 – 0.9 V[17, 18] and the energy loss is generally greater than 0.5 eV.[19-21] Thus, to further improve the OSCs efficiencies, it is necessary to gain insight into the source of the energy loss and then to reduce it further through rational molecular design.

Generally, the energy loss in the OSCs mainly arising from two aspects: the driving force for exciton dissociation and non-radiative recombination. Accordingly, many strategies have been proposed to reduce the energy losses; either by reducing the exciton binding energy by regulating molecular packing, which will minimize the driving force required for exciton dissociation,[22-24] or, by suppressing the non-radiative recombination during the photoelectric conversion processes, such as exciton decay, charge-transfer (CT) state decay and nongeminate (bimolecular) recombination.[25-28] These non-radiative recombinations are all associated with the electron-vibration coupling (namely reorganization energy l, which describes the deformations of the melecular geometries in the course of electron-transfer processe and reflects the interactions between electrons and intramolecular vibrations). Moreover, according to the classical Marcus electron-transfer theory,[29] small reorganization energy facilitate reducing the driving force requried for exciton dissociation. Therefore, the reorganization energy plays a crucial role in the photoelectric conversion and the energy loss processes for OSCs.

In this work, based on the Y-type NFA as the molecular backbone, by replacing thiophene-fused core with quinoxaline (Qx)-fused core, two new small molecule acceptors, Qx-1 and Qx-2 have been designed and synthesised (**Fig. 1a**, and their full names are provided in Supplementary). Historically, Qx and its derivatives have demonstrated various advantages, such as weak electron-deficient properties, rigid plane structures, easy of chemical modification, and multiple substitution positions, which can better regulate their physical and chemical properties.[30-35] Our calculation and experimental results revealed that the reorganization energies during the photoelectric conversion processes of these two acceptors to be substantially smaller than Y6 acceptor, which is beneficial for improved exciton lifetime and diffusion

length, promote charge transport and suppress charge recombination. Consequently, significantly reduced energy losses of 0.508 eV and 0.482 eV for Qx-1 and Qx-2 systems respectively, have been attained, effectively enabling the V_{oc} of both blends to reach over 0.9 V with PM6 (a polymer donor is shown in Supplementary Fig. S1) as a donor. Accordingly, an outstanding PCE of 18.2 % in PM6:Qx-2 blend is obtained with high V_{oc} of 0.934 V, J_{sc} of 26.5 mA cm^{-2} and fill factor (FF) of 73.7%. To the best of our knowledge, the obtained energy loss is the smallest for the binary OSCs with PCEs over 16% reported to date. This work, therefore, underlines the importance of the reorganization energy on achieving small energy loss in organic active materials and paves a new way to obtain high-performance OSCs.

Results And Discussion

2.1. Design, Optoelectronic Characterization and Reorganization Energy

Based on the Y-type NFA as the molecular backbone, by fusing quinoxaline derivatives into the heteraromatic cores, two acceptors named Qx-1 and Qx-2 respectively have been synthesised and their chemical structures are shown in **Fig. 1a**. The detailed synthesis processes and purification methods are listed in Supplementary. These molecules show good solubility and can be dissolved in common solvents, which is beneficial for device fabrication.

The energy levels of Qx-1 and Qx-2 have been estimated from the electrochemical cyclic voltammetry (CV) method and the results are shown in **Fig. 1b**.[36, 37] Compared with Y6 acceptor, both the highest occupied molecular orbital (HOMO) and the lowest unccupied molecular orbital (LUMO) energies of Qx-1 and Qx-2 have been upshifted, resulting in slightly increased bandgaps, owing to the enhanced electron-donating ability of the Qx core-unit as compared with BTZ-based Y6. Therefore, both the energy offset between the HOMOs of donor and acceptor for hole transfer and the LUMOs of donor and acceptor for electron transfer are largely decreased, which further facilitates in reducing the voltage loss of exciton dissociation. The normalized UV-vis absorption spectra of these acceptors in solution and neat films have been shown in **Fig. 1c** (Detailed optical and electrochemical properties of these acceptors are summarized in Supplementary Fig. S2 and Table S1). Since Qx-1 and Qx-2 molecules has a similar molecular backbone, there isn't a significant difference in their absorption data in dilute chloroform solution. Moving from solution to the solid films, their absorption spectra have all been red-shifted, suggesting strong intermolecular π-π interactions.[38] In addition, the Qx-1 exhibits a larger red shift than Qx-2 (ca. 65 nm and 56 nm, respectively), which indicates that the Qx-1 molecules tend to obtain tighter aggregation. It should be noted that these absorption spectra are blue-shifted compared with Y6 molecule, and thus, lead to larger optical bandgaps (E_g^{opt}) for Qx-1 and Qx-2 acceptors. Hence, the higher energy level and larger E_g^{opt} do favor obtaining a higher V_{oc} parameter in the corresponding devices.[39] The absorption and photoluminescence (PL) spectra of Y6, Qx-1 and Qx-2 in the solid films are shown in **Fig. 1d,** which revealed that the stoke's shift between the absorption peak and PL peak of Qx-1 (65 nm) and Qx-2 (68 nm) is significantly smaller than that of Y6 (148 nm). This points out the excited-state relaxations are largely deceased in the Qx-1 and Qx-2 molecules, which is beneficial for reducing the associated voltage losses.

Moreover, to future reveal the molecular packing patterns in the solid state, single crystals of Qx-1 and Qx-2 by solvent diffusion method have been grown and the results are shown in **Fig. 1e-f** (also see Supplementary Fig. S3, Fig. S4 and Table S2). Apparently, both single crystals present one-dimensional arrangements via p-p stacking, which differ from Y6 single crystal with a three-dimensional p-p stacking between adjacent molecules.[24, 40-43] However, in the solid film, the molecular packing is more isotropic, and it is also possible to form a good three-dimensional packing structure.

To further understand the effect of quinoxaline moieties on the electronic structure properties of acceptors, the reorganization energies between different electronic states during photoelectric conversions have been calculated at the tuned-wB97XD/6-31G (d, p) level of theory. As shown in **Fig. 2a** and Table S3 in Supplementary, the reorganization

energy for the S_0 ® S_1 transition ($l_{S0®S1}$) is related to the geometry relaxation in the first excited state (S_1) after light absorption and the reorganization energy for the S_1 ® S_0 transition ($l_{S1®S0}$) is associated with non-radiative exciton decay from the S_1 excitons to the ground state (S_0). Their sum corresponds to reorganization energy for exciton diffusion (l_{EET}, excitation energy transfer). For the exciton dissociation to CT state process, there are two pathways: the dissocation of donor excitons via electron transfer and the dissociation of acceptor excitons via hole transfer. These are corresponding to the reorganization energy for the S_0 ® anion ($l_{S0®anion}$) and S_1 ® anion transitions ($l_{S1®anion}$), respectively. Both of them are related to reorganization energy for exciton dissociation (l_{ED}). In the case of the non-radiative charge recombination (l_{CR}), it is associated with the reorganization energy for the anion ® S_0 transition ($l_{anion®S0}$). The sum of $l_{S0®anion}$ and $l_{anion®S0}$ ultimately, corresponds to the reorganization energy for electron transport.

According to Marcus theory, the smaller the reorganization energy, the smaller the driving force needed for exciton dissociation, and consequently, the faster exciton transfer and charge transport rate. As shown in **Fig. 2b**, compared with Y6, replacing thiophene-fused moiety by quinoxaline-fused moiety leads to a dramatically decrease around 0.02~0.04 eV in the reorganization energy between the S_0 and S_1 transitions. These results indicate that the exciton decay has been suppressed and thus, the quinoxaline-fused moiety helps promote exciton transfer. Moreover, the corresponding calculation results are aslo in good agreement with t the smaller stoke's shifts observed in the experimental measurements for the Qx-1 and Qx-2 systems. Similarly, during the process from exciton dissociation to CT state, it is noted that because of similar geometries of the S_1 and anion states, the reorganization energy for the exciton dissociation via hole transfer ($l_{S1®anion}$) turned out to be very small for all the acceptors. This is again helpful in reducing the voltage loss in the exciton dissociation process. Moreover, the reorganization energy for the exciton dissociation via electron transfer ($l_{S0®anion}$) has also been significantly reduced, which is benificial for obtaining efficient charge generation under a low driving force. In the process from the CT state to charge seperated (CS) state, the CT state decays to the ground state or, recombination of some separated free charge carriers back to the ground state, both processes generally lead to energy losses. Interestingly, the current results reveal the reorganization energies for the transitions between the anion and S_0 states are much smaller for Qx-1 and Qx-2 with respect to Y6, which is benifical to reduce non-radiative recombination loss and promote electron transport.

The reorganization energy can futher be decomposed into contributions from each vibrational mode in the acceptors, the results are shown in **Fig. 2c-f** (the results of Qx-1 are shown in Supplementary Fig. S5). For Y6, there exists one dominated vibrational mode that contributes to the reorganization energy from S_1 to S_0 transition, which corresponds to the stretching of C-C bonds of the central heteraromatic moiety at a high frequency of 1624 cm^{-1}. Interestingly, after fusing quinoxaline derivatives into the heteraromatic cores, this vibration is dramatically inhibited, and thus, facilitates the reduction of exciton decay and promotes exciton transfer. Similarly, in the case of transition from anion to S_0 state, there are four dominated vibrational modes, which include stretching of C-C bonds accompanied by C-H bonds bending at a high frequency above 1500 cm^{-1} (See Supplementary Fig. S6). As seen earlier, these vibrations are significantly suppressed in Qx-1 and Qx-2, resulting in reduced non-radiative recombination and energy loss. Ultimately, these results highlight the importance of reducing the energy loss to improve the efficiency of OSCs by suppressing the C-C bonds stretching.

2.2. Photovoltaic Performance and Energy Loss

The photovoltaic performance of Qx-1 and Qx-2 have been analyzed by fabricating the conventional structure with PM6 as donor (**Fig. 3a**). All detailed optimizing processes are shown in Tables S4-S5 in the Supplementary. The statistical distributions of the best PCEs (*ca.* 30 pieces), density–voltage (*J-V*) characteristics and the external quantum efficiency (EQE) curves of the photovoltaic devices have been provided in **Fig. 3b-3d**. The photovoltaic performance parameters are listed in **Table 1**. Accordingly, by comparing the device performance of the new acceptors with the PM6:Y6 system, a

significant improvement in the Qx-based devices can be observed, as both the Qx-1 and Qx-2 systems demonstrated very high V_{oc} values over 0.9 V. Consequently, the device based on Qx-2 has been able to show an extraordinary PCE of 18.2% with a high V_{oc} of 0.934 V, J_{sc} of 26.5 mA cm^{-2}, and FF of 73.7%. For devices based on Qx-1, on the other hand, the best PCE of 17.9% with a V_{oc} of 0.911 V, J_{sc} of 26.1 mA cm^{-2}, and FF of 75.5% has been attained. To the best of our knowledge, the V_{oc} obtained for Qx-2 devices is the highest for the OSCs with PCE higher than 16% to date (previous work summary in Supplementary Table S6-S7). Furthermore, the integrated current densities from the EQE curves match well with the integrated current density values from the *J*– *V* tests (within the 5% error range), indicating the proposed performance parameters to have good accuracy and reliability. In terms of device stability, the Qx-based devices demonstrated good storage stability in the glove box at room temperature (See Supplementary Fig. S7), as both acceptors can still attain PCEs of 16%, with almost similar V_{oc} and J_{sc} values after being stored for 960 hours.

Table 1. Photovoltaic parameters of OSCs with the donor PM6.

Acceptors	V_{OC} (V)	J_{SC} (mA cm^{-2})	J_{SC}[a] (mA cm^{-2})	FF(%)	PCE(%)
Qx-1	0.911	26.1	24.9	75.5	17.9
	(0.912 ± 0.004)	(25.6 ± 0.3)		(75.4 ± 0.7)	(17.6 ± 0.1)
Qx-2	0.934	26.5	25.3	73.7	18.2
	(0.935 ± 0.004)	(26.0 ± 0.5)		(73.9 ± 1.2)	(17.9 ± 0.2)
Y6	0.859	25.6	24.6	75.3	16.6
	(0.848 ± 0.010)	(25.8 ± 0.3)		(74.6 ± 1.2)	(16.4 ± 0.2)

The average parameters were obtained from 30 independent devices.

The error bars correspond to the standard deviation of 30 independent devices.

[a] The calculated J_{sc} values from the EQE curves.

To probe the charge transport behaviors for the blend films, hole (μ_h) and electron (μ_e) mobilities have been measured by using the space charge limited current (SCLC) method (See Supplementary Fig. S8 and Table S8).[44] The μ_h and μ_e of PM6:Qx-1 blend film came out to be 3.64×10^{-4} and 1.88×10^{-4}, respectively, while the PM6:Qx-2 blend film revealed a μ_h and μ_e of 3.39×10^{-4} and 2.13×10^{-4}, respectively. Compared with PM6:Y6, relatively balanced device mobility has been attained for the new acceptors, and the μ_h /μ_e is 1.94 and 1.59 for Qx-1 and Qx-2, respectively, which is beneficial for the charge transport. Similarly, the effect of charge recombination behavior of these devices has also been explored by measuring the *J*-*V* curves at different light intensities. [45, 46] Consequently, the trap-assisted recombination appears to be suppressed in both Qx-1 and Qx-2-based OSCs (See Supplementary Fig. S9a and S9b). Likewise, to evaluate the exciton dissociation and charge extraction properties, the dependence of the photocurrent density (J_{ph}) on the effective voltage (V_{eff}) of these devices has also been investigated (See Supplementary Fig. S9c).[47] Under short-circuit conditions, the exciton dissociation efficiency for the devices based on Qx-1 and Qx-2 blend turned out to be 97.6% and 97.0%, respectively. Such high exciton dissociation and charge extraction values help in explaining the extremely high J_{sc} and ultimately, high PCE from both systems.

To further gain insight into the high V_{oc} obtained in Qx-based systems, the energy losses (E_{loss}) in both devices have been analyzed. According to the Shockley-Queisser (SQ) limit, the E_{loss} in OSCs can be divided into three parts [16]: $E_{loss} = \Delta E_1 + \Delta E_2 + \Delta E_3$, and the corresponding results have been summarized in **Fig. 3e** and **Table 2**. The ΔE_1 is the inevitable energy loss that depends on the E_g^{pv} of the absorber for a definite solar spectrum and temperature $(\Delta E_1 = E_g - qV_{oc}^{SQ})$, V_{oc}^{SQ} is the output voltage in the SQ limit model. Here, the ΔE_1 value of both Qx-1 and Qx-2 blend films are 0.263 eV, the same as the Y6 blend. The ΔE_2 refers to the radiative recombination loss below the bandgap and is attributed to non-step function absorption $(\Delta E_2 = qV_{oc}^{SQ} - qV_{oc}^{rad} = q\Delta V_{oc}^{rad})$.[48, 49] Because of the presence of CT state in the OSCs, whose energy is usually lower than the optical gap, there is a partial energy loss, which corresponds to the driving force required for exciton dissociation.[50] The measured electroluminescence (EL) spectra of the PM6:Qx-1 and PM6:Qx-2 blend films are very similar to the corresponding neat acceptors without additional emission peaks from the CT states, while the PM6:Y6 blend shows a slightly large redshift as compared to the neat acceptor (See Supplementary Fig. S10). This phenomenon indicates that the energy offsets for exciton dissociation in the PM6:Qx-1 and PM6:Qx-2 blends have largely been reduced. As a result, the ΔE_2 of PM6:Qx-1 and PM6:Qx-2 blend films are around two-fold lower than the PM6:Y6 blend, as small as 0.031 eV and 0.029 eV, respectively. These experimental results are in excellent agreement with the calculations, showing that the reorganization energy for the exciton dissociation in Qx-1 and Qx-2 systems has significantly been reduced, facilitating efficient charge generation at low driving forces.

Similarly, ΔE_3 is the non-radiative recombination $(\Delta E_3 = qV_{oc}^{nonrad} = -k_B T ln(EQE_{EL}))$,

where EQE_{EL} is radiative quantum efficiency of the device when charge carriers are injected in dark conditions. This part of energy loss is ascribed from the non-radiative decay of the CT states to the ground state and the recombination of the separated free charges. As discussed above, when the energy offset between donor and acceptor is small, it will increase the hybridization of the CT state with the highly emissive local excited state, thereby reducing the non-radiative energy loss. Moreover, our calculations show that the reorganization energies for the transitions between the anion and S_0 states are much smaller than for Qx-1 and Qx-2 with respect to Y6, which is beneficial for reducing recombination loss. As a result, the PM6:Qx-1 and PM6:Qx-2 blends exhibit a high EQE_{EL} of 2.53×10^{-4} and 6.60×10^{-4} (See Supplementary Fig. S11), resulting in a small loss of 0.214 eV and 0.190 eV due to the reduced non-radiative recombination, respectively. Since both the driving force required for exciton dissociation and non-radiative recombination have now been significantly reduced, the energy losses in both PM6: Qx-1 and PM6: Qx-2 blend is dramatically decreased, as small as 0.508 eV and 0.482 eV, respectively. Remarkably, the PM6:Qx-2 blend has the lowest energy losses reported to date for the binary OSCs with PCEs over 16% (**Fig. 3f**).

Table 2. Energy loss of the devices based on Qx-1, Qx-2 and Y6 acceptors with PM6 donor.

Devices	a (eV)	EQE_{EL}	qV_{OC}^{SQ} (eV)	qV_{OC}^{rad} (eV)	E_{loss} (eV)	ΔE_1 (eV)	ΔE_2(eV)	ΔE_3(eV)	V_{OC}^{Cal}(V)
PM6:Qx-1	1.420	2.53 ´10^{-4}	1.157	1.120	0.508	0.263	0.031	0.214	0.912
PM6:Qx-2	1.422	6.60 ´10^{-4}	1.159	1.130	0.482	0.263	0.029	0.190	0.941
PM6:Y6	1.419	1.21 ´10^{-4}	1.157	1.091	0.561	0.262	0.066	0.233	0.858

[a] The optical bandgap ( ) was determined from the derivatives of the EQE curve, and a mean peak energy (calculated by the Supplementary equation S13).

2.3. Morphology, Exciton and Charge Dynamics

In addition to rational molecular design, a good phase morphology with moderate phase separation size is also one of the indispensable factors for obtaining high-efficiency OSCs. Here, grazing-incidence wide-angle X-ray scattering (GIWAXS), atomic force microscopy (AFM), transmission electron microscopy (TEM) and resonant soft X-ray scattering (R-SoXS) were used for morphology characterization of the neat and blend films of two acceptors. In the neat films, Qx-1 exhibits stronger crystallization than Qx-2 due to the strong π-π interaction (**Fig. 4a-c**), which is consistent with a higher packing density of single crystal structure of Qx-1 than that of Qx-2. However, in the blend film, Qx-2 exhibits better ability to maintain crystallization than Qx-1(**Fig. 4d-f**). By comparing the corresponding crystal plane parameter between single crystal and GIWAXS of neat films, we can understand the main stacking pattern of Qx-1 and Qx-2 (See Supplementary Fig. S12 and Fig. S13). Compared with the Qx-1 neat films, the stacking mode of (200) as the plane unfavorable charge transfer disappears in the blend films. However, the stacking mode with (002) or (001) and (110) as the plane exist in both the Qx-1 and Qx-2 neat and blend films. These stacking modes indicate the backbone orientation on the substrate is almost vertical, which is conducive to charge transport to the electrodes. Overall, all of the blend films exhibit face-on arrangement and good crystallinity, which facilitate the charge transfer and suppress the charge recombination. Similarly, from the AFM images (See Supplementary Fig. S14), the Qx-1 and Qx-2 blend films exhibit clearly fibrous structure, which favors excellent charge transport and thus, enable the devices to achieve higher J_{sc} and FF.[51, 52] Compared with the results in neat films, the fibrous structure in the blend films is mainly derived from the aggregation characteristics of PM6. Furthermore, the Qx-1 appears to have a more non-planar structure and a poor ability to maintain crystallization, resulting in higher roughness (1.66 nm). On the contrary, the Qx-2 has a planar structure and a better ability to maintain crystallization, resulting in a smaller roughness (0.898 nm). For TEM images of the optimal blend films (See Supplementary Fig. S14), the planar and rigid structure of Qx-2 acceptors is more conducive to breaking the strong self-aggregation of PM6 and obtaining a more uniform phase distribution and smaller domain size, which is consistent with the Resonant Soft X-ray Scattering (R-SoXS) results (See Supplementary Fig. S15). The scattering peaks of the Qx-1 and Qx-2 systems are at q = 0.07 and 0.15 nm^{-1} respectively, indicating that the phase domain size of the Qx-2 system (21.63 nm) is smaller than the Qx-1 system (43.56 nm). This phase size is the relatively ideal active layer morphology of OSCs and thus facilitates in achieving higher exciton dissociation and charge transport efficiency.

Apart from film morphology, the investigation of exciton and charge dynamics can give us a deeper understanding of the exciton transport and charge generation behavior in the active layer. Hence, the time-resolved photoluminescence (TRPL) spectrum of neat and blended films has been carried out to determine the exciton lifetime, and the results are shown in **Fig. 4g**. Thus, the exciton lifetime of both Qx-1 and Qx-2 neat films (863.1 ps and 690.4 ps, respectively) turned out to be greater than Y6 (679.2 ps). In addition, the quantum yield (QY) of Qx-2 (12.34%) and Qx-1(7.365%) also came out to be

higher than Y6 (6.42%, see Supplementary Table S9). These results point out that Qx-1 and Qx-2 have a lower exciton decay than Y6. Likewise, an obvious fluorescence quenching in the blends as compared to the lifetime of the neat film has also been observed, indicating an efficient exciton dissociation, especially for the PM6:Qx-2 system (See Supplementary Fig. S16). The exciton-exciton annihilation (EEA) method has future been used to investigate the exciton diffusion length (L_D).[53, 54] The calculated L_D of Qx-1 and Qx-2 turned out to be comparable to Y6, as values 10.6 nm, 9.5 nm and 12.6 nm for Y6, Qx-1 and Qx-2, respectively (See supplementary Fig. S17 and Table S10). These results are also in accordance with the previous ones and dictate that reducing the reorganization energy is an effective pathway to suppress exciton decay and improve the exciton transport and lifetime.

The photo-induced CT behavior has further been investigated by measuring the Transient absorption spectrum (TAS) of the neat and blend films (See Supplementary Fig. S18 and Fig. S19). A beam of 400 nm and 800 nm excitation light has been used to form PM6 donor excitons and Qx-1 and Qx-2 acceptor excitons, respectively. The negative signals in the range from 600 to 650 nm have been assigned to the ground state bleach (GSB) of PM6. Meanwhile, a GSB peak at 825 nm is observed that matches the absorption spectrum of acceptors. Since the absorption spectra of the donor and acceptors can be well separated, the hole transfer dynamics can be clearly investigated by selectively exciting the acceptor molecules. The pump wavelength of 800 nm is set to excite the acceptors in the blend film. Accordingly, an additional GSB peak has been observed at 630 nm that attributed to the PM6 donor, resulting from the ultrafast hole transfer from Qx-1 and Qx-2 acceptor to the donor at the donor-acceptor interface. In addition, both PM6:Qx-2 and PM6:Qx-1 blends exhibit a much faster hole transfer rate than Y6, which benefits the effective charge generation in the OSCs **(Fig. 4h)**. These results are in good agreement with the high-performance of two Qx-based blends.

Conclusions

In this work, two new acceptors of Qx-1 and Qx-2 with bigger volume and higher rigid BTP as central core have been synthesized. It has been observed that by suppressing the molecular vibration of stretching of C-C bonds in both acceptors, we find that the reorganization energies during the photoelectric conversions have significantly reduced as compared to the converntional Y6 acceptor. Thus, the energy losses arising from the exciton dissociation and non-radiative recombination have greatly been reduced. Hence, a relationship between the reorganization energy and the energy losses has been well established. Furthermore, the film morphology, exciton and charge dynamics results prove the Qx-1 and Qx-2 acceptors with smaller reorganization energy have better aggregation patterns, better exciton lifetime and longer diffusion lengths, contributing to the effective charge generation in corresponding OSCs. As a result, the PM6:Qx-1 blend produced a PCE of 17.9% with an energy loss of 0.508 eV, whereas the PM6:Qx-2 system attained an outstanding PCE of 18.2% with an energy loss of 0.482eV, significantly outperforming its Y6 counterpart. To the best of our knowledge, the obtained energy loss is the smallest for the binary OSCs with PCEs over 16% reported to date. This work underlines the importance of the reorganization energy for achieving small energy loss in organic active materials and thereby provides a new strategy towards the high performance of OSCs.

Methods

Materials. The synthetic route of acceptors Qx-1 and Qx-2 is illustrated in Scheme 1 in Supplementary. Polymer donor PM6 were purchased from Solar Materials. The detailed synthetic procedures of Qx-1 and Qx-2 and the corresponding structural characterizations can be found in the Supplementary.

Single-crystal growth. Single crystal of Qx-1 and Qx-2 were grown by the liquid diffusion method at room temperature. An appropriate amount of methanol is transferred to a concentrated chloroform solution, which will form crystals over time. Single crystal diffraction was collected at low temperatures protected by liquid nitrogen in accordance with standard procedures for reducing X-ray radiation damage through use the single crystal X-ray diffractometer (model is XtaLAB

PRO 007HF(Mo), manufactured by Rigaku). The X-ray crystallographic coordinates for structures reported of Qx-1 and Qx-2 have been deposited at the Cambridge Crystallographic Data Centre (CCDC), under deposition numbers 2120380–2120381.

UV-vis absorption. Measured by Perkin Elmer Lambda 950 spectrophotometer.

Electrochemical cyclic voltammetry (CV). Measured with an electrochemical workstation (VMP3 Biologic, France) with a Pt disk coated with blend film, a Pt plate, and an Ag^+/Ag electrode acting as the working, counter, and reference electrodes, respectively, in a 0.1mol/L tetrabutylammonium phosphorus hexafluoride (Bu_4NPF_6) acetonitrile solution.

Device fabrication and measurement. All the PSC devices were fabricated by using an conventional structure of ITO/PEDOT:PSS/PM6:acceptors/PNDIT-F3N-Br/Ag, where PNDIT-F3N-Br (poly[(9,9-bis(3'-((N,N-dimethyl)-N-ethylammonium)propyl)-2,7 fluorene)-alt-5,5'-bis(2,2'-thiophene)-2,6-naphthalene-1,4,5,8-tetracaboxylic-N,N'-di(2ethylhexyl)imide]dibromide) and PEDOT:PSS (poly(3,4-ethylenedioxythiophene:poly(styrenesulfonate)) were respectively used as electron-transport and hole-transport interlayer. The blended solution was prepared by mixing PM6 and acceptors into chloroform with the addition of a small amount of chloronaphthalene (0.6 %, v/v), the mix solution was stirred at 50 °C in chloroform for 1.5 h until they dissolved. The optimal device conditions of Qx-1 and Qx-2 were prepared by mixing donor and acceptors in a 1:1.5 and1:1.3 weight ratio, respectively, into chloroform with the addition of a small amount of 1-chloronaphthalene (0.6 %, v/v) and under thermal annealing at 100 °C and 110°C for 10 min, respectively.

A solar simulator was used for *J–V* curves measurement under AM 1.5 G ($100mWcm^{-2}$). Newport Oriel PN 91150 V Sibased solar cell was applied for light intensity calibration. *J–V* measurement signals were recorded by a Keithley 2400 source-measure unit. The device area of each cell was approximately $4mm^2$. And the measurements were performed by scanning voltage from -1.5 to 2 V with a voltage step of 10 mV and delay time of 1ms. Oriel Newport system (Model 66902) equipped with a standard Si diode was used for EQEs test in air condition.

Mobility measurements. The electron mobility was acquired with the device structure of Al/active layer or neat acceptors/PNDIT-F3N-Br/Al, the hole mobility was obtained by preparing the structure of ITO/PEDOT:PSS/active layer/MoOx/Ag. The current density-voltage (*J-V*) curves in the range of 0-5 V were obtained by a Keithley 2420 Source-Measure Unit in the dark.

Energy loss. Highly sensitive EQE was measured using an integrated system (PECT-600, Enlitech), where the photocurrent was amplified and modulated by a lock-in instrument. EQE_{EL} measurements were performed by applying external voltage/current sources through the devices (ELCT-3010, Enlitech). EQE_{EL} measurements were performed for all devices according to the optimal device preparation conditions.

Morphology characterization. Transmission electron microscopy (TEM) images were acquired on Tecnai G2 F20 U-TWIN TEM instrument. The atomic force microscopy (AFM) characterization was performed by Bruker Multimode 8 in ScanAsyst Mode in air. Grazing incidence wide angle x-ray scattering (GIWAXs) measurement was conducted at the beamline of 7.3.3 at the Advanced Light Source (ALS). Resonant Soft X-ray Scattering (R-SoXS): R-SoXS transmission measurements were performed at beamline 11.0.1.2 at the Advanced Light Source (ALS).

Exciton and Charge Dynamics. The excitation and emission spectra, the time-resolution photoluminescence (TRPL) spectrum and absolute quantum yield (QY) test by transient/steady state fluorescence spectrometer, manufactured by Edinburgh Instruments, model number is FLS1000. The PL spectrum of film and solution use a xenon lamp to excite the light source, use 750nm pump for film excitation, and use 600nm pump for solution excitation. Absolute quantum yield using an integrating sphere and a blank quartz plate as a reference to measure the absolute quantum yield. TA

measurements were performed on an Ultrafast Helios pump-probe system in collaboration with a regenerative amplified laser system from Coherent.

Declarations

Acknowledgements

This work was financially supported by National Natural Science Foundation of China (Grant Nos. 22073020, 21822503, 51973043, 21773040, 22135001, 21721002, 51961135103) and the Strategic Priority Research Program of the Chinese Academy of Sciences (No. XDB36000000).

Author contributions

Y.S. synthesized and characterized the NFAs of Qx-1 and Qx-2. Y.C. and Y.Y. performed the device fabrication and characterization. Y.S. tested the energy loss data. L.Z. carried out theoretical calculations. Y.S. and L.Z. grew the single crystals and analyzed the single-crystal structures of Qx-1 and Qx-2. Z.C. and X.H. measured and analyzed transient absorption spectroscopy. J.Z. measured and analyzed the GIWAXS. D.Q. and Y.L. performed the TEM measurements of the single crystal. Y.S. performed the morphology characterization and analyzed the data. W.M. performed the R-SoXS measurements. Adil. modify the language. Z.W., K.L. and L.Z. supervised the project, Y.S., L.Z., K.L., and Z.W. wrote the paper.

References

1. S. Gunes, H. Neugebauer&N. S. Sariciftci Conjugated polymer-based organic solar cells *Chem. Rev.* **107**, 1324-1338 (2007).

2. G. Li, et al. High-efficiency solution processable polymer photovoltaic cells by self-organization of polymer blends *Nat. Mater.* **4**, 864-868 (2005).

3. J. B. Zhao, et al. Efficient organic solar cells processed from hydrocarbon solvents *Nat. Energy* **1**, 15027 (2016).

4. J. H. Hou, O. Inganas, R. H. Friend&F. Gao Organic solar cells based on non-fullerene acceptors *Nat. Mater.* **17**, 119-128 (2018).

5. G. Li, R. Zhu&Y. Yang Polymer solar cells *Nature Photon.* **6**, 153-161 (2012).

6. J. Yuan, et al. Fused Benzothiadiazole: A Building Block for n-Type Organic Acceptor to Achieve High-Performance Organic Solar Cells *Adv. Mater.* **31**, e1807577 (2019).

7. J. Yuan, et al. Single-junction organic solar cell with over 15% efficiency using fused-ring acceptor with electron-deficient core *Joule* **3**, 1140-1151 (2019).

8. R. Qin, et al. Tuning terminal aromatics of electron acceptors to achieve high-efficiency organic solar cells *J. Mater. Chem. A* **7**, 27632-27639 (2019).

9. J. Yuan, et al. Enabling low voltage losses and high photocurrent in fullerene-free organic photovoltaics *Nat. Commun.* **10**, 1624 (2019).

10. C. Li, et al. Non-fullerene acceptors with branched side chains and improved molecular packing to exceed 18% efficiency in organic solar cells *Nat. Energy* **6**, 605-613 (2021).

11. L. Meng, et al. Organic and solution-processed tandem solar cells with 17.3% efficiency *Science* **361**, 1094-1098 (2018).

12. Y. Cui, et al. Single-Junction Organic Photovoltaic Cell with 19% Efficiency *Adv. Mater.* **33**, 2102420 (2021).

13. K. Yoshikawa, et al. Silicon heterojunction solar cell with interdigitated back contacts for a photoconversion efficiency over 26% *Nat. Energy* **2**, 17032 (2017).

14. Z. Liu, et al. Open-Circuit Voltages Exceeding 1.26 V in Planar Methylammonium Lead Iodide Perovskite Solar Cells *ACS Energy Lett.* **4**, 110-117 (2018).

15. J. Yuan, et al. Reducing Voltage Losses in the A-DA'D-A Acceptor-Based Organic Solar Cells *Chem.* **6**, 2147-2161 (2020).

16. J. Z. Yao, et al. Quantifying Losses in Open-Circuit Voltage in Solution-Processable Solar Cells *Phys. Rev. Appl.* **4**, 014020 (2015).

17. L. Hong, et al. Eco-Compatible Solvent-Processed Organic Photovoltaic Cells with Over 16% Efficiency *Adv. Mater.* **31**, e1903441 (2019).

18. S. Liu, et al. High-efficiency organic solar cells with low non-radiative recombination loss and low energetic disorder *Nature Photon.* **14**, 300-305 (2020).

19. D. Qian, et al. Design rules for minimizing voltage losses in high-efficiency organic solar cells *Nat. Mater.* **17**, 703-709 (2018).

20. Y. N. Shi, et al. Optimizing the Charge Carrier and Light Management of Nonfullerene Acceptors for Efficient Organic Solar Cells with Small Nonradiative Energy Losses *Sol. RRL* **5**, 2100008 (2021).

21. J. X. Pan, et al. pi-Extended Nonfullerene Acceptors for Efficient Organic Solar Cells with a High Open-Circuit Voltage of 0.94 V and a Low Energy Loss of 0.49 eV *ACS Appl. Mater. Interfaces* **13**, 22531-22539 (2021).

22. L. Zhu, Z. Tu, Y. Yi&Z. Wei Achieving Small Exciton Binding Energies in Small Molecule Acceptors for Organic Solar Cells: Effect of Molecular Packing *J. Phys. Chem. Lett.* **10**, 4888-4894 (2019).

23. L. Zhu, C. Yang, Y. Yi&Z. Wei Effective Modulation of Exciton Binding Energies in Polymorphs of a Small-Molecule Acceptor for Organic Photovoltaics *J. Phys. Chem. Lett.* **11**, 10227-10232 (2020).

24. L. Zhu, J. Zhang, Y. Guo, C. Yang, Y. Yi&Z. Wei Small Exciton Binding Energies Enabling Direct Charge Photogeneration Towards Low-Driving-Force Organic Solar Cells *Angew. Chem. Int. Ed.* **60**, 15348-15353 (2021).

25. J. Benduhn, et al. Intrinsic non-radiative voltage losses in fullerene-based organic solar cells *Nat. Energy* **2**, 17053 (2017).

26. D. Qian, et al. Design rules for minimizing voltage losses in high-efficiency organic solar cells *Nat. Mater.* **17**, 703-709 (2018).

27. G. Han, Y. Yi&Z. Shuai From Molecular Packing Structures to Electronic Processes: Theoretical Simulations for Organic Solar Cells *Adv. Energy Mater.* **8**, 1702743 (2018).

28. S. M. Menke, N. A. Ran, G. C. Bazan&R. H. Friend Understanding Energy Loss in Organic Solar Cells: Toward a New Efficiency Regime *Joule* **2**, 25-35 (2018).

29. R. A. Marcus Electron transfer reactions in chemistry. Theory and experiment *Rev. Mod. Phys.* **65**, 599-610 (1993).

30. C. K. Sun, C. Zhu, L. Meng&Y. F. Li Quinoxaline-Based D-A Copolymers for the Applications as Polymer Donor and Hole Transport Material in Polymer/Perovskite Solar Cells *Adv. Mater.* 2104161 (2021).

31. Z. Y. Zhang, et al. Novel conjugated polymers with planar backbone bearing acenaphtho 1,2-b quinoxaline acceptor subunit for polymer solar cells *Synth. Met.* **175**, 21-29 (2013).

32. Z. C. Zhou, et al. Subtle Molecular Tailoring Induces Significant Morphology Optimization Enabling over 16% Efficiency Organic Solar Cells with Efficient Charge Generation *Adv. Mater.* **32**, 1906324 (2020).

33. W. R. Liu, J. Y. Zhang, S. J. Xu&X. Z. Zhu Efficient organic solar cells achieved at a low energy loss *Sci. Bull.* **64**, 1144-1147 (2019).

34. F. Liu, et al. Organic Solar Cells with 18% Efficiency Enabled by an Alloy Acceptor: A Two-in-One Strategy *Adv. Mater.* **33**, 2100830 (2021).

35. Y. Y. Zhao, et al. Fine-tuning the energy levels and morphology via fluorination and thermal annealing enable high efficiency non-fullerene organic solar cells *Mater. Chem. Front.* **4**, 3310-3318 (2020).

36. Q. J. Sun, H. Q. Wang, C. H. Yang&Y. F. Li Synthesis and electroluminescence of novel copolymers containing crown ether spacers *J. Mater. Chem.* **13**, 800-806 (2003).

37. H. Bin, et al. 11.4% Efficiency non-fullerene polymer solar cells with trialkylsilyl substituted 2D-conjugated polymer as donor *Nat. Commun.* **7**, 13651 (2016).

38. S. Badgujar, et al. High-Performance Small Molecule via Tailoring Intermolecular Interactions and its Application in Large-Area Organic Photovoltaic Modules *Adv. Energy Mater.* **6**, 1600228 (2016).

39. M. Erray, M. Hanine, E. Boufounas&A. El Amrani Combined effects of carriers charge mobility and electrodes work function on the performances of polymer/fullerene P3HT:PCBM based organic photovoltaic solar cell *Eur. Phys. J-Appl. Phys.* **82**, 30201 (2018).

40. C. Xiao, C. Li, F. Liu, L. Zhang&W. Li Single-Crystal Field-Effect Transistors based on a Fused-Ring Electron Acceptor with High Ambipolar Mobilities *J. Mater. Chem. C* **8**, 5370 (2020).

41. L. Zhu, et al. Efficient Organic Solar Cell with 16.88% Efficiency Enabled by Refined Acceptor Crystallization and Morphology with Improved Charge Transfer and Transport Properties *Adv. Energy Mater.* **10**, 1904234 (2020).

42. G. Zhang, et al. Delocalization of exciton and electron wavefunction in non-fullerene acceptor molecules enables efficient organic solar cells *Nat. Commun.* **11**, 3943 (2020).

43. W. Zhu, et al. Crystallography, Morphology, Electronic Structure, and Transport in Non-Fullerene/Non-Indacenodithienothiophene Polymer:Y6 Solar Cells *J. Am. Chem. Soc.* **142**, 14532-14547 (2020).

44. P. W. M. Blom, M. J. M. deJong&J. J. M. Vleggaar Electron and hole transport in poly(p-phenylene vinylene) devices *Appl. Phys. Lett.* **68**, 3308-3310 (1996).

45. L. J. Koster, M. Kemerink, M. M. Wienk, K. Maturova&R. A. Janssen Quantifying bimolecular recombination losses in organic bulk heterojunction solar cells *Adv. Mater.* **23**, 1670-4 (2011).

46. A. K. Kyaw, et al. Intensity dependence of current-voltage characteristics and recombination in high-efficiency solution-processed small-molecule solar cells *ACS Nano* **7**, 4569-77 (2013).

47. G. Li, et al. Efficient modulation of end groups for the asymmetric small molecule acceptors enabling organic solar cells with over 15% efficiency *J. Mater. Chem. A* **8**, 5927-5935 (2020).

48. D. B. Yang, Y. M. Wang, T. Sano, F. Gao, H. Sasabe&J. Kido A minimal non- radiative recombination loss for efficient non- fullerene all- small- molecule organic solar cells with a low energy loss of 0.54 eV and high open- circuit voltage of 1.15 V+ *J. Mater. Chem. A* **6**, 13918-13924 (2018).

49. R. Zhou, et al. All-small-molecule organic solar cells with over 14% efficiency by optimizing hierarchical morphologies *Nat. Commun.* **10**, 5393 (2019).

50. K. Vandewal, J. Benduhn&V. C. Nikolis How to determine optical gaps and voltage losses in organic photovoltaic materials *Sustain. Energy Fuels* **2**, 538-544 (2018).

51. H. Fu, Z. Wang&Y. Sun Polymer Donors for High-Performance Non-Fullerene Organic Solar Cells *Angew. Chem. Int. Ed. Engl.* **58**, 4442-4453 (2019).

52. T. Liu, et al. Optimized Fibril Network Morphology by Precise Side-Chain Engineering to Achieve High-Performance Bulk-Heterojunction Organic Solar Cells *Adv. Mater.* **30**, e1707353 (2018).

53. A. Classen, et al. The role of exciton lifetime for charge generation in organic solar cells at negligible energy-level offsets *Nat. Energy* **5**, 711-719 (2020).

54. Y. Firdaus, et al. Long-range exciton diffusion in molecular non-fullerene acceptors *Nat. Commun.* **11**, 5520 (2020).

Figures

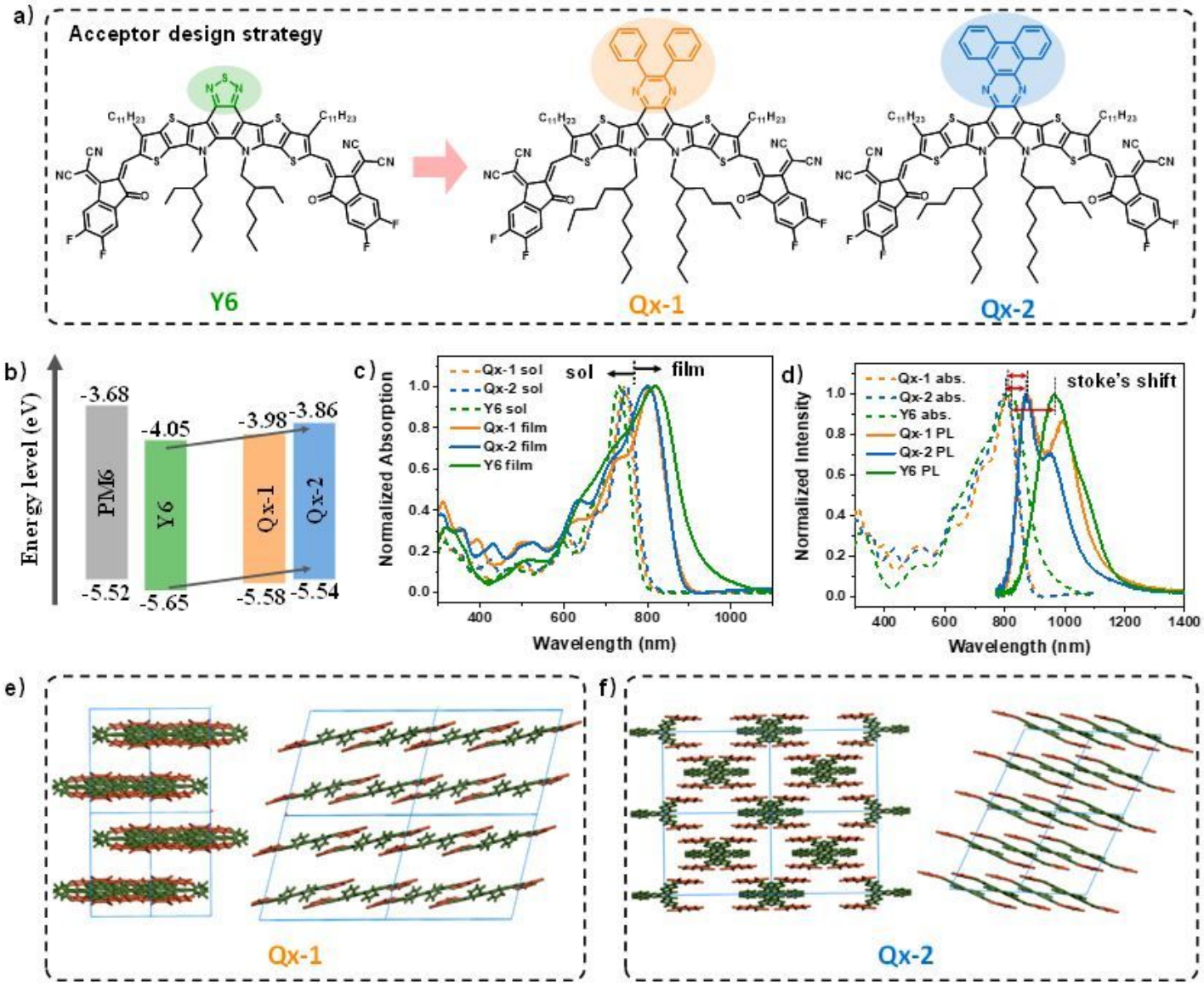

Figure 1

(a) Chemical structures of Qx-1 and Qx-2 acceptors and PM6 polymer donor. (b) Energy level diagram of the related materials. (c) UV-vis absorption spectra of the acceptors in the solution and film. (d) UV-vis absorption and photoluminescence (PL) spectra of acceptors in the film. (e-f) The molecular packing patterns of Qx-1 and Qx-2 in the single crystal structure.

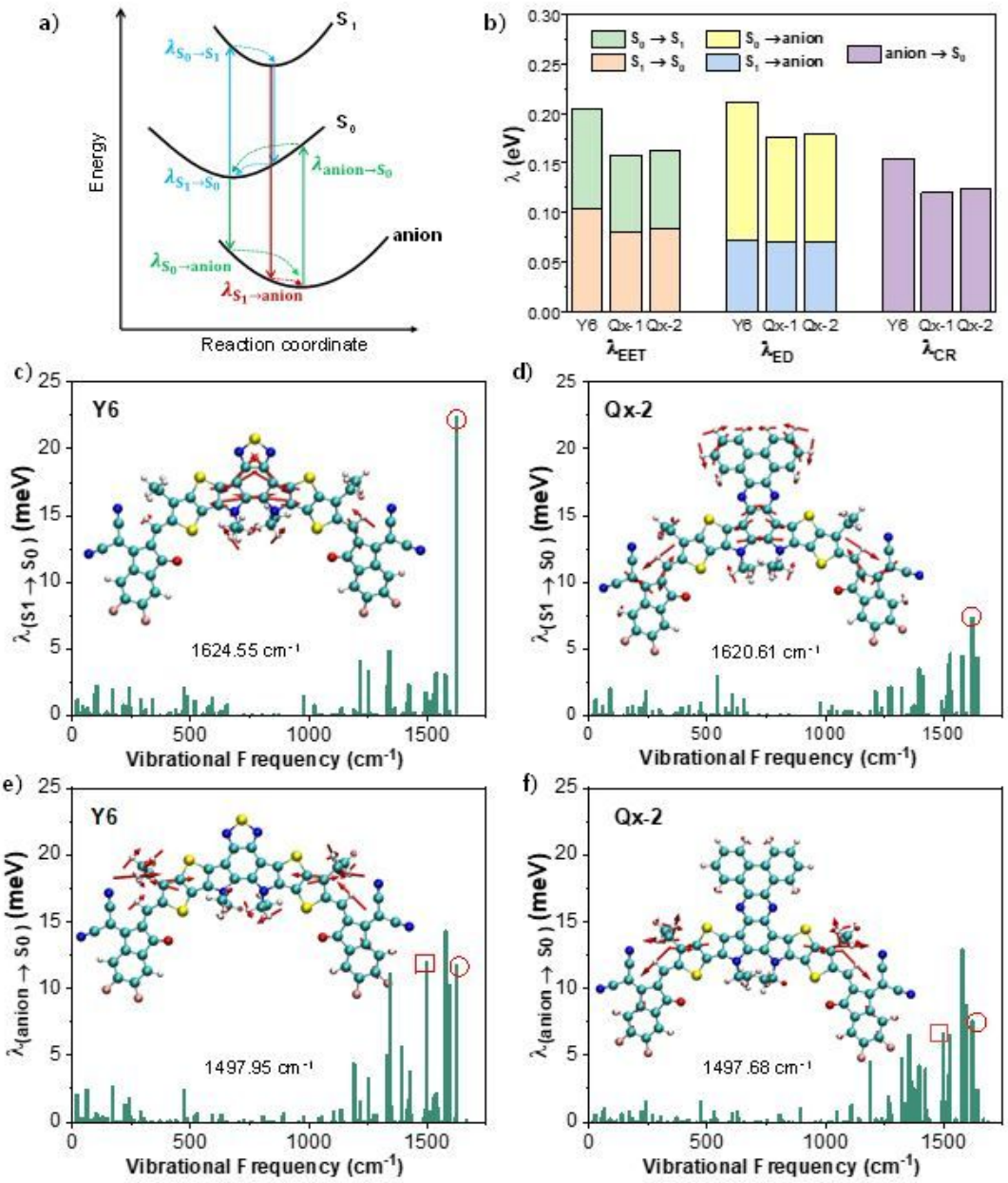

Figure 2

(a) Illustration of the related transitions among the ground state (S_0), the lowest singlet excited state (S_1), and the anionic state during the photoelectric conversion processes, taking the acceptor as an example. (b) the calculated reorganization energies for the mutual transitions between the different electronic states at the level of wB97XD/6-31G(d,p) with tuned w values in Y6, Qx-1 and Qx-2 acceptors. (c-f) Contributions of each vibrational mode to the reorganization energy for the S_1 ® S_0 and anion ® S_0 transiitons of Y6 and Qx-2. Illustration of the displacement vectors for the vibrational normal modes marked by circles (at around 1625 cm^{-1}) and squares (at around 1498 cm^{-1}) are inserted. The length of displacement vectors stands for the magnitude of vibrational strength.

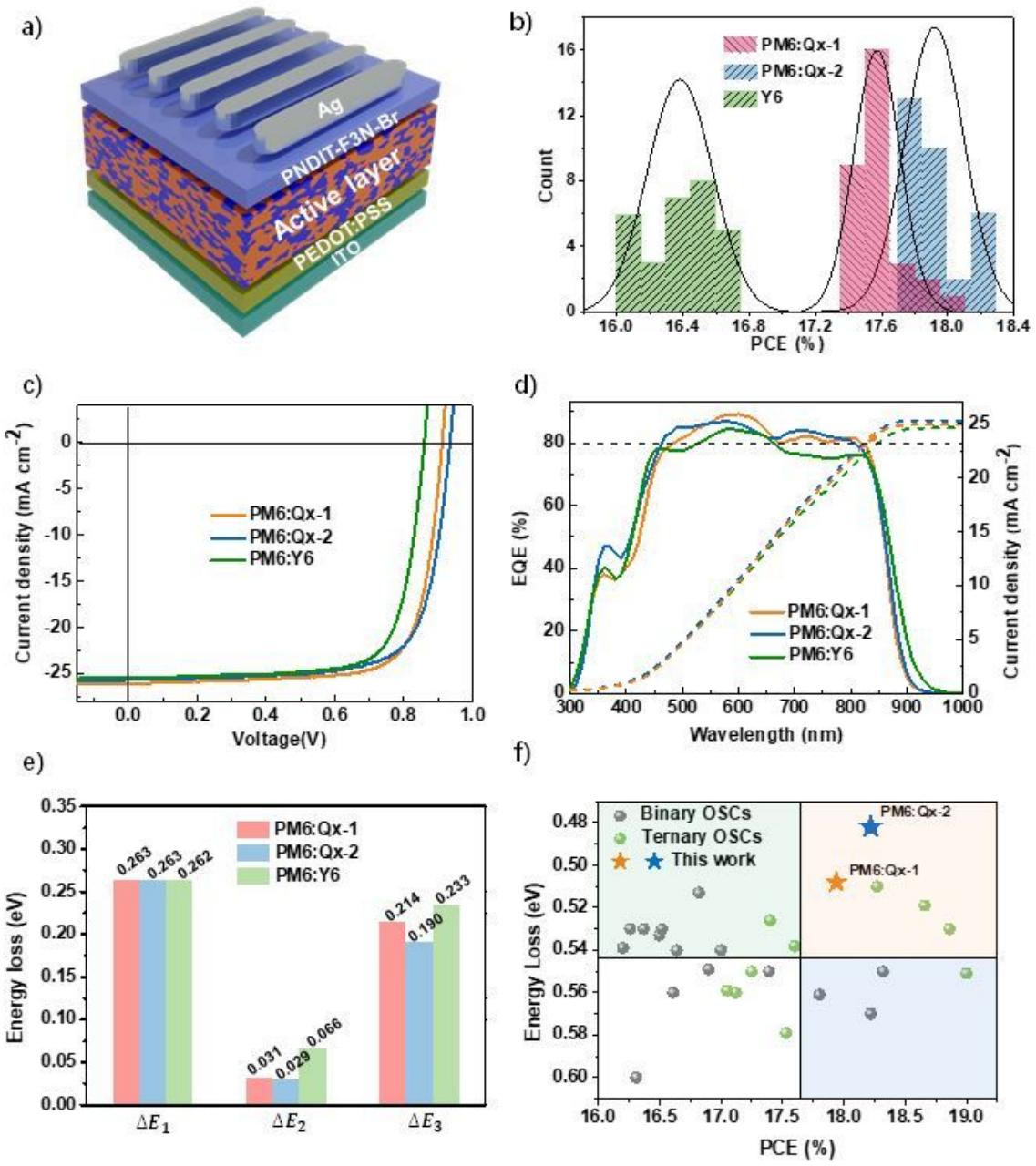

Figure 3

Photovoltaic performance and energy loss of Qx-1, Qx-2 and Y6 with PM6 as the donor. (a)The conventional device architecture; (b) Statistics distribution of best PCE for *ca.*30 pieces; (c) The density–voltage (*J-V*) curves; (d)The external quantum efficiency (EQE) spectra and the integrated current densities from the EQE spectra of the optimal device; (e) Statistical diagram of energy loss; (f) Plots of the PCE against energy loss for various systems.

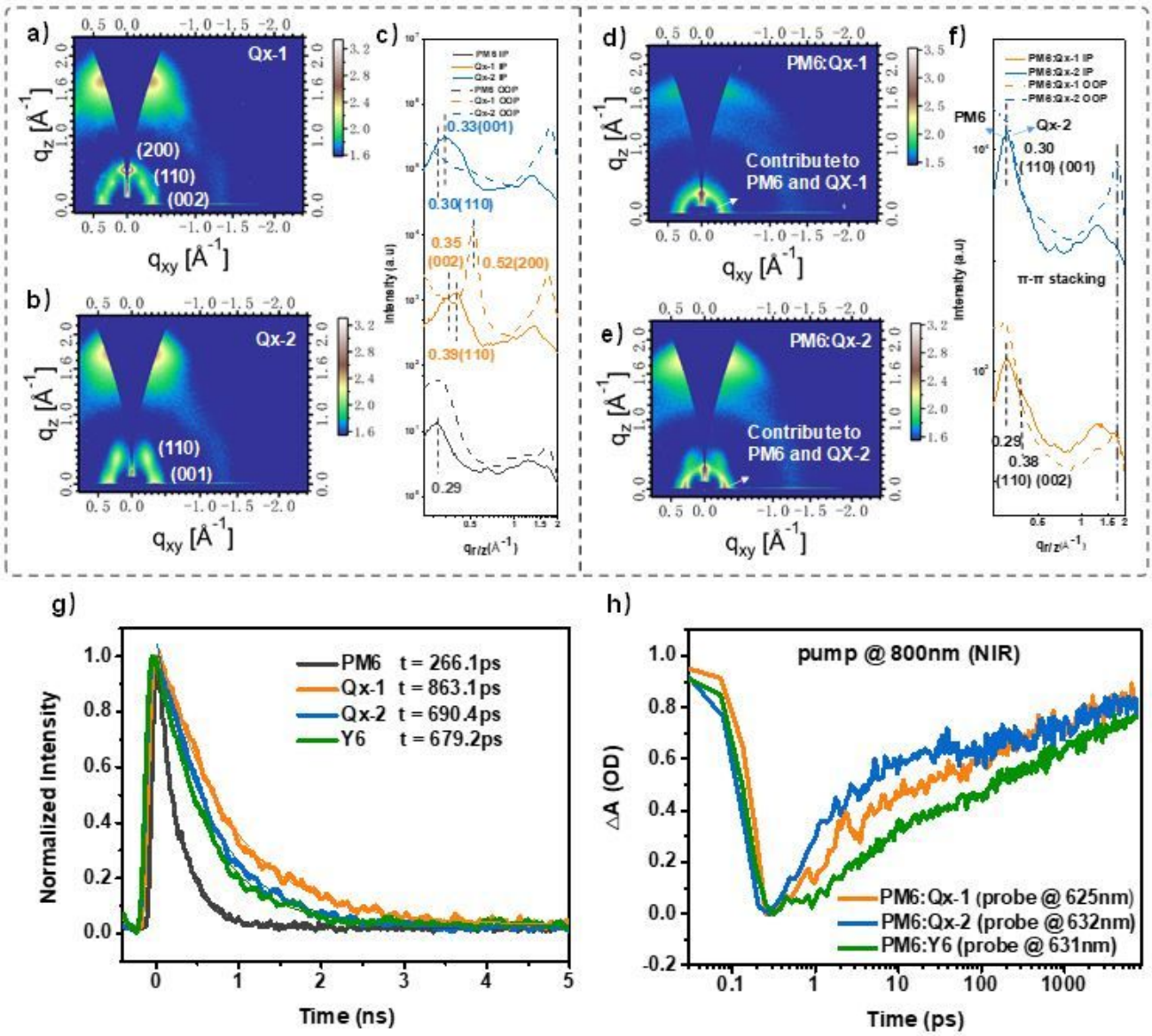

Figure 4

(a-c) Two-dimensional GIWAXS patterns and in-plane and out-of-plane cuts of the neat films of Qx-1 and Qx-2 acceptors; (e-f) Two-dimensional GIWAXS patterns and in-plane and out-of-plane cuts of blend films; (g) Time-resolution photoluminescence (TRPL) spectrum of donor and acceptors in neat films; (h) Transient kinetic traces of PM6 GSB probing at around 630 nm for the blend films.

Supplementary Files

This is a list of supplementary files associated with this preprint. Click to download.

- QxNatureEnergySI20211202.docx
- SolarCellsReportingSummary.pdf